Thermochimica Acta 552 (2013) 137–141

Contents lists available at SciVerse ScienceDirect

Thermochimica Acta

journal homepage: www.elsevier.com/locate/tca

Experimental evaluation and thermodynamic assessment of the LiF–LuF_3 phase diagram

I.A. dos Santos [a,*], D. Klimm [b], S.L. Baldochi [a], I.M. Ranieri [a]

[a] Instituto de Pesquisas Energéticas e Nucleares, CP 11049, Butantã 05422-970, São Paulo, SP, Brazil
[b] Leibniz Institute for Crystal Growth, Max-Born-Straße 2, 12489 Berlin, Germany

ARTICLE INFO

Article history:
Received 10 May 2012
Received in revised form 30 October 2012
Accepted 2 November 2012
Available online xxx

Keywords:
Phase diagrams
Computer simulation
Characterization
Rare earth compounds

ABSTRACT

The phase diagram of the system LiF–LuF_3 has been revised using thermal analysis. Specific heat capacity and enthalpy of phase transition and fusion were measured by differential scanning calorimetry for all compounds belonging to the system. A thermodynamic optimization of the LiF–LuF_3 phase diagram was performed by fitting the Gibbs energy functions to the experimental data that were taken from the literature or measured in this work. Excess energy terms, which describe the effect of interaction between the two fluoride compounds in the liquid solution, were expressed by the Redlich–Kister polynomial function. The assessed phase diagram was in suitable agreement with the re-evaluated experimental data.

1. Introduction

$LiLuF_4$ (LLF) crystals have been largely investigated for doping with optically active rare earth ions, mainly focusing on the development of laser media [1–5]. Taking into account that LLF has the most compact crystalline structure among the $LiREF_4$ (RE = rare earth element or *Y*, respectively) crystals family, some studies have also reported the $Li(Lu,RE)F_4$ (RE = Gd or *Y*) mixed crystals as an alternative to achieve better optical properties, either wider emission bandwidths [6,7] or improvement of their photochemical stability [8].

Conversely, there is a lack of information concerning the thermodynamic properties of LLF and the corresponding LiF–LuF_3 phase diagram. Heat capacity and enthalpy data for LuF_3 were initially investigated by Spedding et al. [9] and, more recently, Lyapunov et al. revised the enthalpy data and proposed a new $C_P(T)$ function for this compound [10]. No thermodynamic data are available for LLF whilst LiF data are given by the Barin compilation [11].

The phase diagram of the system LiF–LuF_3 was initially studied in the 1960s by Thoma et al. [12], who reported the stability of only one intermediate compound (LLF), melting congruently at 1098 K, and taking part in two eutectic reactions together with the terminal components LiF and LuF_3. The liquid compositions and the temperatures of these eutectic reactions were reported to be placed at: (i) 22 mol% LuF_3 and 968 K for the LiF-rich eutectic, and (ii) 54 mol% LuF_3 and 1083 K for the LuF_3-rich eutectic. The polymorphic transition from orthorhombic to hexagonal structure in LuF_3 was reported at 1218 K. Harris et al. [13] revised this phase diagram in the 1980s, determining the melting point of LLF at 1123 K, the LiF-rich eutectic was reported at 20 mol% LuF_3 and 977 K and the LuF_3-rich eutetic at 58 mol% LuF_3 and 1105 K. Both group of authors used thermal analysis to determine the invariant reactions and respective temperatures. In this work, the LiF–LuF_3 binary system was experimentally revised through DSC technique. The enthalpy of phase transition and fusion for all compounds which belong to this system were calculated. Using the obtained data and those collected from literature [10,11,14], LiF–LuF_3 phase diagram has been optimized. The excess Gibbs energy terms for the liquid solution, which describe the interaction effects between the two fluorides, were expressed by the Redlich–Kister polynomial function [15]. Enthalpy of formation and entropy at 298.15 K were assessed for LuF_3 and LLF.

2. Experimental

The samples utilized to construct the LiF–LuF_3 phase diagram were prepared from commercial LiF (AC Materials, 99.999%) and LuF_3 (AC Materials, 99.99%). Samples (mass around 3 g) with different compositions were prepared by weighing appropriate quantities of LiF and LuF_3 powder that were homogenized in a mortar. DSC curves were obtained using a Netzsch STA 409 PC Luxx heat-flux differential scanning calorimeter. The sample carrier was calibrated for *T* and sensitivity at the phase transformation points of $BaCO_3$ and at the melting temperatures of In, Zn and Au. The experiments were carried out under Ar flow of 30 cm^3/min, using

* corresponding author.

0040-6031/$ – see front matter © 2012 Elsevier B.V. All rights reserved.
http://dx.doi.org/10.1016/j.tca.2012.11.015

Pt/Au crucibles with lid. Two heating/cooling cycles with temperature variation rate of 10 K/min and samples masses around 30 mg were adopted. The melting point of the compounds, the temperature of the solid phase transition and of the invariant reactions were calculated considering the extrapolated onset of the thermal events on heating. The liquidus temperatures of the intermediate compositions were evaluated from the extrapolated offset temperatures.

The heat capacity measurements were performed using the same equipment described above, where a proper sample carrier for C_P analysis was installed. The experiments consisted of three steps, an isothermal segment at 40 °C for 20 min, a dynamic heating segment with heating rate of 10 K/min and a final isothermal segment at maximum temperature for 5 min. Other experimental conditions were kept as mentioned previously for simple DSC experiment. LuF_3 and $LiLuF_4$ heat capacity were determined according to the ratio method. In this method, the sample DSC heat flow signal is compared to the DSC signal of a calibration standard of known specific heat (sapphire in this case). Both curves are corrected by a baseline correction experiment where empty reference and sample crucibles are placed in the DSC furnace and the system signal drift is measured under identical experimental conditions.

3. Thermodynamic method

A thermodynamic simulation of a $T-X$ binary phase diagram requires the description of Gibbs energy functions for all compounds in the system and the Gibbs functions of mixing, if solution phases are present. In most cases the excess Gibbs functions are unknown for the solutions, therefore a thermodynamic assessment is necessary in order to determine thermal effects of mixing. Gibbs energy for a solid compound is defined as a function of enthalpy and entropy at the reference temperature state (298.15 K) and can be obtained from the heat capacity function ($C_P(T)$) as follows:

$$C_P(T) = a + bT + cT^{-2} \tag{1}$$

$$H(T) = H^0_{298.15\,K} + \int_{298.15\,K}^{T} C_P\,dT \tag{2}$$

$$S(T) = S^0_{298.15\,K} + \int_{298.15\,K}^{T} \frac{C_P}{T}\,dT \tag{3}$$

Combining the Eqs. (2) and (3), the $G(T)$ equation is given as follows:

$$G(T) = H^0_{298.15\,K} - (S^0_{298.15\,K})T + \int_{298.15\,K}^{T} C_P\,dT - T\int_{298.15\,K}^{T} \frac{C_P}{T}\,dT \tag{4}$$

Usually the heat capacity is the most accessible physical property to be measured. $C_P(T)$ functions can be determined by fitting a set of experimental data at a proper polynomial function (*e.g.* Eq. 1). Depending on the compound, more terms are added or disregarded in the polynomial function to obtain the best fitting. According to Eq. (1) and considering the Eqs. (2) and (3), the enthalpy of formation, the absolute entropy at the reference temperature and the heat capacity are required to determine the minimum of G and thus the thermodynamic equilibrium. These data are not available for the LLF, therefore the experimental data calculated by DSC were assumed to set the C_P equation. Also, the experimental C_P data were compared with the Neumann–Kopp rule (NKR), which is an empirical rule for the estimation of temperature dependence of heat capacity of mixed compounds [16]. The C_P equation for LuF_3 was estimated using the data obtained by DSC technique and the result was compared with the literature values. Enthalpy and entropy at 298.15 K for LLF were properly assessed by optimization. The thermodynamic data for the LiF and LuF_3 end members were taken from Barin compilation [11] or from [10,14]. Table 1 summarizes all calorimetric data used on the phase diagram assessment.

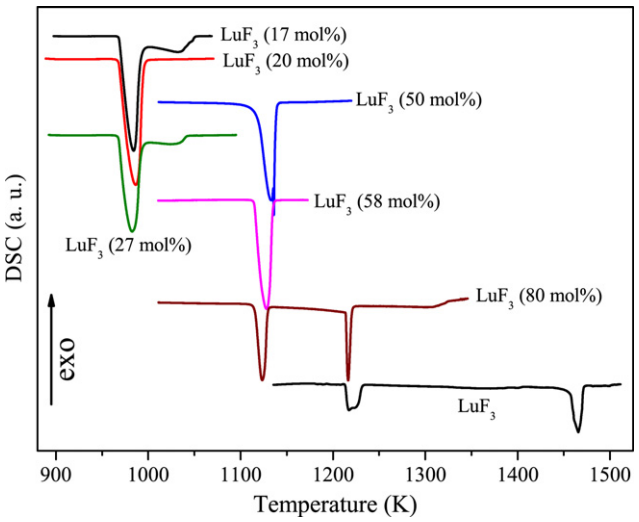

Fig. 1. Second heating DSC curves for some compositions in the LiF–LuF_3 system.

For the liquid solution phase, function $G(T)$ is expressed as the sum of the Gibbs energy weighed contribution of the pure compounds (G_0), the contribution of an ideal mixture (G_{ID}) and finally a term related to the non-ideal interaction, defined as the excess energy (G_{ex}). The sub-regular solution model of Redlich–Kister was adopted to describe the excess energy of the liquid phase in this system [15], and is given by:

$$G_{ex} = x_A x_B \sum_{j=0}^{N} L_j (x_A - x_B)^j \tag{5}$$

where x_A and x_B are the molar fractions of components A and B, respectively. L_j terms represent the interaction coefficients between the basis compounds and they are given as a linear function of temperature. The optimization was performed using the OptiSage module in the FactSage 6.2 software [17], which uses the Bayesian Algorithm [18]. This algorithm is based on a probability model to obtain the fit between the theoretical Gibbs energy functions and the experimental data.

4. Results and discussion

4.1. Experimental results

DSC curves for pure LuF_3 and six different compositions are shown in Fig. 1. The curves for 17, 20 and 27 mol% LuF_3 exhibit one endothermic peak with onset near to 968 K. This peak is due to the L $\rightleftharpoons$ LiF+$LiLuF_4$ eutectic, and the 20 mol% LuF_3 DSC curve shows a single peak at this temperature, since the eutectic point is very close to this composition. The second broader endothermic peaks at 17 and 27 mol% LuF_3 curves mark the end of melting of the primary phase (LiF and $LiLuF_4$ respectively) at the liquidus.

Curves with compositions of 50 and 58 mol% illustrate the LLF congruent melting at 1126 K, and the second eutectic reaction at 1115 K, respectively. DSC curve for 80 mol% LuF_3 shows, beyond the small peak representing the liquidus line, also two intermediate peaks with onset at 1115 K and 1216 K corresponding to the second eutectic reaction and the LuF_3 polymorphic transition from orthorrombic to hexagonal, respectively.

Table 1
ΔH(298.15 K) (kJ ,mol per formula unit), S(298.15 K) (J ,K mol per formula unit), ΔH_{PT} (Phase transition: heat of fusion or polymorphic transition) (kJ ,mol per formula unit) and C_P data a, b, c entering Eq. (1) for LiF, LuF_3 and the intermediate compound $LiLuF_4$.

Compound	ΔH(298.15 K)	S(298.15 K)	ΔH_{PT} (Lit)	ΔH_{PT}[a]	a	b	c
LiF(S)[b]	−616.931	35.660	27.09	27.68	42.689	1.742×10^{-2}	-5.301×10^{5}
LiF(l)[b]	−598.073	43.441	–	–	64.183	–	–
LuF_3($S1$)[a]	−1681.000[c]	94.830[c]	25.40[d]	18.28	97.496	9.460×10^{-3}	-9.998×10^{5}
LuF_3($S2$)[a]	−1674.290	89.350	29.90[d]	23.34	114.500[d]	–	–
LuF_3(l)[a]	−1671.014	77.904	–	–	131.800[d]	–	–
$LiLuF_4$[a]	−2316.129	128.624	–	63.538	139.430	3.200×10^{-2}	-1.881×10^{6}

[a] ΔH_{PT} and C_P function were measured by the DSC technique; ΔH(298.15 K) and S(298.15 K) were assessed in this work.
[b] Data taken from Barin [11].
[c] Data taken from Flotow et al. [14].
[d] Data taken from Lyapunov et al. [10].

Table 2
Experimental and calculated invariant points in the LiF–LuF_3 phase diagram and the previously reported data.

	Composition (Mol % LuF_3)				Temperature (K)			
Equilibrium Reaction	Exp.	Calc.	Thoma [12]	Harris [13]	Exp.	Calc.	Thoma [12]	Harris [13]
L ⇌ LiF+LLF (Eutectic)	20	21.5	22	20	968	967.0	968	977
L ⇌ LLF (Congruent melting)	50	50.0	50	50	1126	1123.3	1098	1123
L ⇌ LLF+LuF_3($S1$) (Eutectic)	58	57.1	54	58	1115	1116.6	1083	1105
L+LuF_3($S1$) ⇌ L+LuF_3($S2$) (Polymorphic transition)	–	–	–	–	1216	1216.0	1218	–

Finally, in the LuF_3 curve the polymorphic transition (1216 K) and fusion (1457 K) can be recognized very clearly. The main features of the LiF–LuF_3 experimental phase diagram are summarized in Table 2 together with some previously reported data. In general, the data obtained in this work are in agreement with those from Harris et al. phase diagram [13].

The heat of fusion and polymorphic transition (ΔH_{PT}) for LiF, LuF_3 and $LiLuF_4$ were calculated from the DSC peak area of these thermal effects for each compound. In a previous work, the experimental ΔH_{PT} for LiF was reported and reasonable agreement with the literature value was found [11,19]. Compared to the literature data, the main difference in the results were noticed for LuF_3 thermal events. The evaluated ΔH_{PT} for LuF_3 in this work are approximately 20 % smaller than those reported by Lyapunov et al. [10]. Since our DSC experiments were repeatedly confirmed and the raw materials used were very pure, these new results have been taken into account to the final calculation of the LiF–LuF_3 phase diagram. The heat of fusion and heat capacity ($C_P(T)$ function) for the $LiLuF_4$ compound have not yet been reported in the literature. Therefore, for the first time these calorimetric properties were evaluated. Fig. 2 compares the C_P data calculated through DSC technique and those estimated using the corresponding $C_P(T)$ functions of the end member compounds and considering the Neumann–Kopp rule. One can see, for the considered temperature range, that there are no signicant deviations (not bigger than 3%) between the experimental and estimated C_P data. Furthermore, taking into account the polynomial fitting of the DSC experimental data using function (1), the a, b and c parameters obtained define the $C_P(T)$ function for the $LiLuF_4$ compound.

Heat capacity re-evaluation for the LuF_3 orthorhombic phase (LuF_3(S1)) was also carried out by DSC (Fig. 3). The first C_P data reported for this compound were deduced from enthalpy measurements for temperatures above 400 K by Spedding et al. [9]. Later, Flotow et. al. [14] measured C_P data for the LuF_3(S1) phase from low temperature up to 400 K. Lastly, Lyapunov et al. [10] proposed a $C_P(T)$ function for this low temperature phase taking into account enthalpy measurements as well. Comparing the results obtained by DSC measurements with those previously reported, one can notice reasonable agreement, considering both experimental data and the fitted $C_P(T)$ function. It is worth to remark that the $C_P(T)$ function proposed in this work could be extrapolated to represent the heat

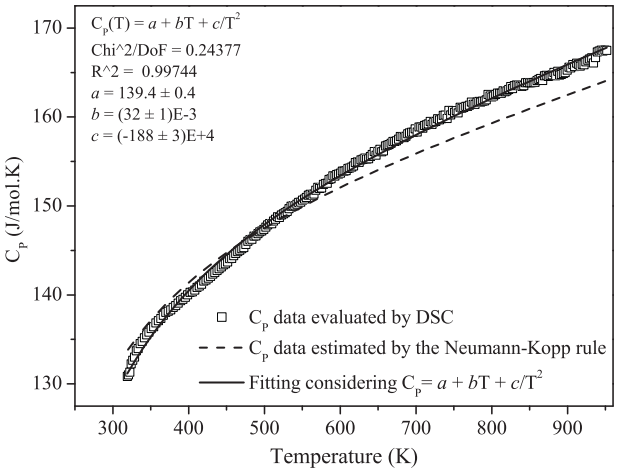

Fig. 2. $LiLuF_4$ C_P data experimentally measured through DSC technique and C_P function estimated by the Neumann–Kopp rule. These data are also available in the Supplementary data section.

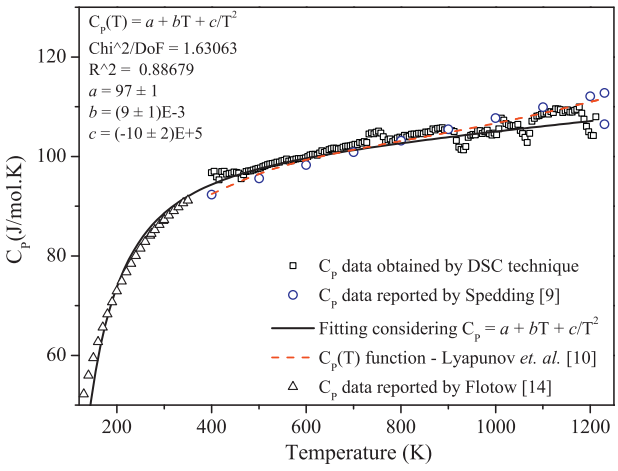

Fig. 3. LuF_3 C_P data experimentally obtained through DSC technique compared with those previously reported by Sppeding et al. [9], Flotow et al. [14] and the $C_P(T)$ function proposed by Lyapunov et al. [10]. The primary DSC data are also available in the Supplementary Data section.

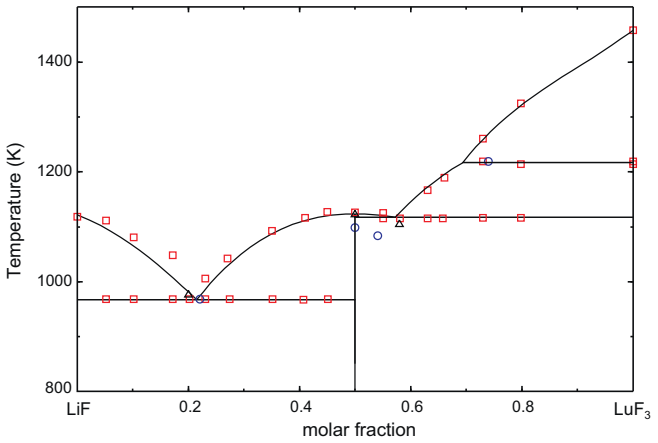

Fig. 4. Assessed phase diagram of the system LiF–LuF_3 (lines) together with the experimental data from DSC (□) and those from literature: ○ – Thoma et al.[12] and △ – Harris et al. [13].

capacity from the room temperature up to the polymorphic transition temperature of LuF_3, since it was found good agreement relative to Flotow data at 298.15 K. Some small deviations from the general behavior of the curve were observed for the DSC measured C_P data (*e.g.* 930 and 1065 K). Those undesirable effects are due to small fluctuations on the DSC baseline and they can be disregarded. Taking that aside, the difference between the evaluated and the reported data is not larger than 4%, even for the higher temperatures considered. Therefore, the $C_P(T)$ parameters set by fitting a polynomial model (1) on DSC experimental data were assumed to perform the numerical optimization in the LiF–LuF_3 system.

4.2. Thermodynamic assessment

Once the $T-X$ experimental points are available and the calorimetric data for each compound belonging to the system were evaluated or collected from the literature, a proper optimization of the LiF–LuF_3 phase diagram became possible. The excess Gibbs energy for liquid phase has been optimized according to the Redlich–Kister polynomial model using the Bayesian Optimization Algorithm of FactSage [17].

Fig. 4 presents the LiF–LuF_3 optimized phase diagram together with the $T-X$ experimental points for comparison. It may be highlighted an excellent agreement of the assessed temperature values for the eutectic reactions, LuF_3 polymorphic transition and even for the liquidus line. $LiLuF_4$ congruent melting point was confirmed at ~1123 K. The value calculated for LiF/$LiLuF_4$ eutectic composition was about only 1 mol% larger than the experimental value. However, it should be noted that close thermal events are rather hard to separate, as the case of liquids and solidus lines near the eutectic composition. In general, the experimental determination of the liquidus from offsets is much less accurate than the determination of the eutectic or phase transition temperatures. The assessed enthalpy and entropy at 298.15 K for the LuF_3 (hexagonal and liquid phases) and for $LiLuF_4$, are listed in Table 1. The calculated excess parameters, given by L_0 and L_1 in the Redlich–Kister model (Eq. 5) were $L_0 = -36329.71 + 7.26T$ and $L_1 = 4573.25 + 13.86T$. Even though those numbers can not be taken as the only possible, they represent the best assessment achieved. Together with the other data presented in this work, that numerical simulation gives a complete thermodynamic description for the LiF–LuF_3 phase diagram.

5. Conclusions

Thermodynamic assessment has been performed on the LiF–LuF_3 binary system and the excess Gibbs energy terms for the liquid phase could be properly optimized using the Redlich–Kister polynomial model. Based on our experimental results and the thermodynamic assessment it was possible to confirm the values for the two eutectic temperatures within this system. A $C_P(T)$ function of $LiLuF_4$ compound has been set for the first time and it was in accord with Neumann–Kopp rule. It has been successfully confirmed the previously C_P data found in the literature for LuF_3 (orthorhombic phase). ΔH(298.15 K) and S(298.15 K) have been assessed for LuF_3 (hexagonal and liquid phases) and $LiLuF_4$, and a re-evaluation for ΔH_{PT} data in the LuF_3 compound was performed. This work offers a more complete thermodynamic description of LiF–LuF_3 system and makes further thermodynamic assessments possible for ternary and multi component phase diagram based on this binary one.

Acknowledgments

The authors acknowledge financial support from CAPES (Grant no. 368/11) and DAAD (Grant no. po-50752632) in the framework of the PROBRAL program, and from CNPq (477595/2008-1). One of the authors (I.A. dos Santos) acknowledges financial support from DAAD-CAPES-CNPq (290111/2010-2). This work also was supported by the EU Commission in the Seventh Framework Programme through the ENSEMBLE project (Grant Agreement Number NMP4-SL-2008-213669).

Appendix A. Supplementary Data

Supplementary data associated with this article can be found, in the online version, at http://dx.doi.org/10.1016/j.tca.2012.11.015.

References

[1] A.F.H. Librantz, L. Gomes, L.G.V. Tarelho, I.M. Ranieri, Investigation of the multiphoton excitation process of $4f^2 5d$ configuration in $LiYF_4$ and $LiLuF_4$ crystals doped with trivalent neodymium ion, J. Appl. Phys 95 (2004) 1681–1691.
[2] A.F.H. Librantz, L. Gomes, S.L. Baldochi, I.M. Ranieri, G.E. Brito, Luminescence study of the $4f^2 5d$ configuration of Nd^{3+} in $LiYF_4$, $LiLuF_4$ and BaY_2F_8 crystals, J. Lumin. 121 (2006) 137–148.
[3] H.J. Strauss, W. Koen, C. Bollig, M.J.D. Esser, C. Jacobs, O.J.P. Collett, D.R. Preussler, Ho:YLF and Ho:LuLF slab amplifier system delivering 200 mJ, 2μm single-frequency pulses, Opt. Express 19 (15) (2011) 13974–13979.
[4] S.J. Shu, T. Yu, R.T. Liu, J.Y. Hou, X. Hou, W.B. Chen, Diode-side-pumped AO Q-switched Tm:Ho:LuLF laser, Chinese Opt. Lett. 9 (9) (2011) 091407.
[5] F. Cornacchia, A. Richter, E. Heumann, G. Huber, D. Parisi, M. Tonelli, Visible laser emission of solid state pumped $LiLuF_4:Pr^{3+}$, Opt. Express 15 (2007) 992–1002.
[6] I.A. dos Santos, R. Bertram, L. Gomes, S.L. Baldochi, I.M. Ranieri, Growth and characterization of the $LiGd_{0.25}Lu_{0.75}F_4$ crystal doped with neodymium, J. Phys.: Conf. Ser. 249 (2010) 01–07.
[7] N.D. Vieira Jr., I.M. Ranieri, L.V.G. Tarelho, N.U. Wetter, S.L. Baldochi, L. Gomes, P.S.F. de Matos, W. de Rossi, G.E.C. Nogueira, L.C. Courrol, E.A. Barbosa, E.P. Maldonado, S.P. Morato, Laser development of rare-earth doped crystals, J. Alloys Compd. 344 (2002) 231–239.
[8] A.S. Nizamutdinov, V.V. Semashko, A.K. Naumov, S.L. Korableva, R.Y. Abdulsabirov, A.N. Polivin, M.A. Marisov, Optical and gain properties of series of crystals LiF-YF_3-LuF_3 doped with Ce^{3+} and Yb^{3+} ions, J. Lumin. 127 (2007) 71–75.
[9] F.H. Spedding, D.C. Henderson, High-temperature heat contents and related thermodynamic functions of seven trifluorides of the rare earths Y, La, Pr, Nd, Gd, Ho and Lu, J. Chem. Phys. 54 (1971) 2476–2483.
[10] K. Lyapunov, A. Baginskii, S. Stankus, Experimental study of the enthalpy of lutetium trifluoride in solid and liquid states, J.Alloys Compd. 372 (2004) 7–9.
[11] I. Barin, Thermodynamic Data of Pure Substances, VCH, Weinheim, 1993.
[12] R.E. Thoma, G.D. Brunton, R.A. Penneman, T.K. Keenan, Equilibrium relations and crystal structure of lithium fluorolanthanate phases, Inorg. Chem. 9 (1970) 1096–1101.
[13] I.R. Harris, H. Safi, N.A. Smith, M. Altunbas, B. Cockayne, J.G. Plant, The relationship between crystal growth behavior and constitution in the systems LiF–LuF_3, LiF–ErF_3 and LiF–YF_3, J. Mater. Sci. 18 (1983) 1235–1243.
[14] H.E. Flotow, P.A.G. O'Hare, Thermodynamics of the lanthanide trifluorides. IV. The heat capacities of gadolinium trifluoride GdF_3, lutetium trifluoride LuF_3, and yttrium trifluoride YF_3 from 5 to 350 K, J. Chem. Phys. 74 (1981) 3046–3055.

[15] O. Redlich, A.T. Kister, Algebraic representation of thermodynamic properties and the classification of solutions, Ind. Eng. Chem. 40 (1948) 345–348.
[16] J. Leitner, P. Voňka, D. Sedmidubský, P. Svoboda, Application of Neumann–Kopp rule for the estimation of heat capacity of mixed oxides, Thermochim. Acta 497 (2010) 7–13.
[17] GTT Technologies,;1; Kaiserstr. 100, 52134 Herzogenrath, Germany, FactSage 6.2, http://www.factsage.com/ (2010).
[18] M. Pelikan, D.E. Goldberg, E. Cantu-Paz, The Bayesian optimization algorithm, in: W. Banzhaf, J. Daida, A.E. Eiben, M.H. Garzon, V. Honavar, M. Jakiela, R. Smith (Eds.), Proceedings of the Genetic and Evolutionary Computation Conference GECCO-99, 1999, pp. 525–532.
[19] I.A. dos Santos, D. Klimm, S.L. Baldochi, I.M. Ranieri,;1; Thermodynamic modeling of the LiF–YF_3 phase diagram, J. Crystal Growth http://dx.doi:10.1016/j.jcrysgro.2011.11.009